PAPER

Optical second-harmonic generation of Janus MoSSe monolayer

To cite this article: Ce Bian *et al* 2022 *Chinese Phys. B* **31** 097304

Optical second-harmonic generation of Janus MoSSe monolayer

Ce Bian(边策)[1,2], Jianwei Shi(史建伟)[3,4], Xinfeng Liu(刘新风)[3,4], Yang Yang(杨洋)[1], Haitao Yang(杨海涛)[1,2,5,†], and Hongjun Gao(高鸿钧)[1,2,5]

[1] *Beijing National Laboratory for Condensed Matter Physics and Institute of Physics, Chinese Academy of Sciences, Beijing* 100190, *China*
[2] *School of Physical Sciences, University of Chinese Academy of Sciences, Chinese Academy of Sciences, Beijing* 100190, *China*
[3] *CAS Key Laboratory of Standardization and Measurement for Nanotechnology and CAS Center for Excellence in Nanoscience, National Center for Nanoscience and Technology, Beijing* 100190, *China*
[4] *School of Nanoscience and Technology, University of Chinese Academy of Sciences, Beijing* 100049, *China*
[5] *Songshan Lake Materials Laboratory, Dongguan* 523808, *China*

(Received 10 March 2022; revised manuscript received 23 April 2022; accepted manuscript online 7 May 2022)

The transition metal dichalcogenides (TMD) monolayers have shown strong second-harmonic generation (SHG) owing to their lack of inversion symmetry. These ultrathin layers then serve as the frequency converters that can be intergraded on a chip. Here, taking MoSSe as an example, we report the first detailed experimental study of the SHG of Janus TMD monolayer, in which the transition metal layer is sandwiched by the two distinct chalcogen layers. It is shown that the SHG effectively arises from an in-plane second-harmonic polarization under paraxial focusing and detection. Based on this, the orientation-resolved SHG spectroscopy is realized to readily determine the zigzag and armchair axes of the Janus crystal with an accuracy better than $\pm 0.6^\circ$. Moreover, the SHG intensity is wavelength-dependent and can be greatly enhanced (~ 60 times) when the two-photon transition is resonant with the C-exciton state. Our findings uncover the SHG properties of Janus MoSSe monolayer, therefore lay the basis for its integrated frequency-doubling applications.

Keywords: Janus MoSSe monolayer, second-harmonic generation (SHG), orientation-resolved spectroscopy, C-exciton resonance

PACS: 73.63.Bd, 42.70.Mp, 42.65.Ky, 42.79.Nv **DOI:** 10.1088/1674-1056/ac6db4

1. Introduction

As a nonlinear optical process, the second-harmonic generation (SHG) converts two photons of the fundamental frequency ω to a single photon of the harmonic frequency 2ω.[1] This frequency-doubling process is of vital importance to the current laser technology, such as laser generations in blue and green regions.[2] To realize this nonlinear optical sourcing on a chip, the SHG of two-dimensional (2D) materials has been extensively studied.[3,4] Of particular interest are the transition metal dichalcogenide (TMD) monolayers which exhibit strong SHG owing to their lack of inversion symmetry.[5–8] The SHG intensity can be further controlled through electrostatic gating,[9,10] and its polarization characteristic is sensitive to mechanical strain.[11–13] In addition, the integrations of TMD monolayer with quantum dots,[14] nanowires,[15,16] and optical cavities[17–20] offer an SHG platform that possesses reduced dimension and diverse functionalities.

The realization of Janus TMD monolayers in 2017 greatly enriches the TMD family.[21,22] The peculiar Janus structure — different chalcogen species on the different faces — leads to unusual excitonic dynamics (e.g., long radiative recombination lifetime)[23,24] and novel optoelectronic applications (e.g., photovoltaic cell with high power conversion efficiency).[25] However, the feasibility and performance of such a monolayer as the frequency-doubling medium have been less explored. Here, taking MoSSe as an example, we report the first detailed experimental study of the SHG of Janus TMD monolayer. Though the second-harmonic polarization has both in- and out-of-plane components, the SHG effectively arises from an in-plane reduced polarization when considering paraxial focusing and detection. An orientation-resolved SHG spectroscopy can be realized in terms of the reduced polarization and Jones calculus, which determines the zigzag and armchair directions of the Janus crystal to an accuracy better than $\pm 0.6^\circ$. Moreover, by tuning the excitation at the C-exciton resonance, the SHG intensity can be greatly enhanced by a factor of ~ 60, which implies a nearly eight-fold increase of the second-order susceptibility $\chi^{(2)}_{yyy}$. Our results demonstrate that the Janus MoSSe monolayers is a tunable nonlinear medium in the 2D limit, which is potentially suited for the on-chip frequency-doubling applications.

2. Methods

Janus MoSSe monolayer was converted from MoS_2 monolayer via the graphene-assisted bottom-face substitution (see Figs. S1 and S2 in the supplementary materials for details). The resulting sample is a vertical heterostructure in which the Janus MoSSe monolayer is encapsulated by few-layered graphene. Raman and photoluminescence (PL) characterizations were performed by a commercial equipment

†Corresponding author. E-mail: htyang@iphy.ac.cn

(WITec alpha 300R) under the 532-nm laser excitation. Power and wavelength dependences of SHG were measured by a home-built system equipped with a tunable femtosecond laser source (Coherent Chameleon Ultra Ⅱ) and liquid-nitrogen-cooled charge-coupled-device (CCD) detector (Princeton Instrument Acton SP2500i). As for the orientation-resolved SHG measurements, a 1064-nm polarized picosecond laser source (NPI Rainbow 1064 OEM) was connected to a commercial equipment (WITec alpha 300RA). A motorized half-wave plate was placed in the common optical path to rotate the polarizations of both input laser and output SHG. A linear polarizer was inserted in front of the spectrometer entrance as the analyzer. Linear absorption spectra were acquired by a home-built system equipped with a tungsten-halogen white-light source (Thorlabs SLS201L) and a thermoelectric-cooled CCD detector (HORIBA iHR 550). The spectra were calculated with $(I_0 - I)/I_0$, where I and I_0 represent the signal intensities at the sample and the bare SiO_2/Si substrate, respectively. For all optical measurements, the light source was focused by a 100× microscope objective with the numerical aperture (NA) of 0.9, which subsequently collected the signal in the backscattering geometry.

3. Results and discussion

The atomic structure of a Janus MoSSe monolayer is illustrated in Fig. 1(a). The out-of-plane mirror symmetry is lifted by the sulfur and selenium atoms that locate on the opposite faces. Raman spectroscopy was used to verify the Janus structure of as-converted samples. As shown in Fig. 1(b), the spectrum of Janus MoSSe monolayer exhibits the characteristic bands A_1^1 and E^2 at ~ 290 and ~ 354 cm^{-1}, respectively, in clear contrast to those of pristine MoS_2 monolayer (A_1' and E' at ~ 406 and ~ 382 cm^{-1}, respectively).[26,27] The full width at half maximum (FWHM) of A_1^1 band is similar to those of A_1' and E' bands (~ 6 cm^{-1}), therefore the high crystal quality has been retained after the Janus conversion. Additionally, as shown in Fig. 1(c), the PL spectra exhibit the redshift from ~ 1.85 eV (MoS_2) to ~ 1.72 eV (MoSSe), which is consistent with the reported change of the A-exciton emission.[28]

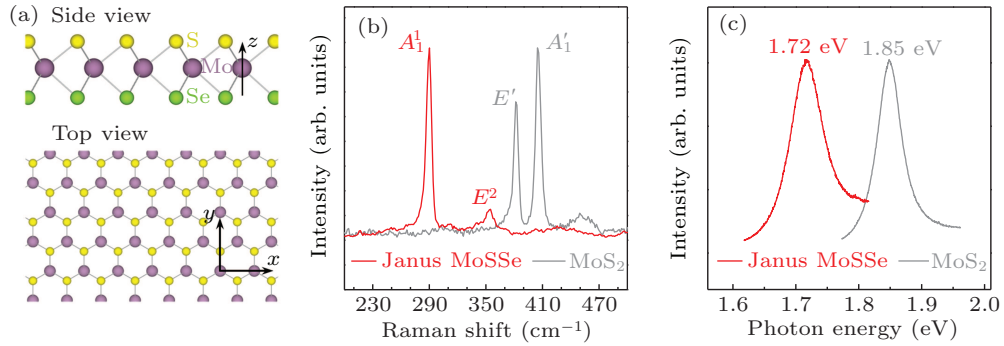

Fig. 1. (a) Atomic structure of Janus MoSSe monolayer. The definitions of Cartesian indices are overlaid. (b) and (c) Raman and PL characterizations of the as-converted Janus MoSSe monolayer, respectively. The normalized spectra of pristine MoS_2 monolayer are also shown for comparison.

The nonlinear optical response of Janus MoSSe monolayer was probed using an 800-nm excitation, and the second-harmonic emission at 400 nm was detected (Fig. 2(a)). Since SHG is a second-order process, its intensity scales quadratically with the excitation power.[29] This relation is clearly shown on a log–log scale (Fig. 2(b)). The linear fitting yields the slope of ~ 2.2, which is close to the theoretical value of 2. The deviation could be explained by the measurement uncertainties under low excitation powers. However, photodamage occurs as the excitation power continuously increases, resulting in a reduction of SHG intensity and hence the slope (see Fig. S3 in the supplementary materials).[30] To avoid the photodamage, laser power has been carefully adjusted during other measurements. In addition, the SHG microscopy confirms that the detected signal arises from the Janus MoSSe monolayer, while no signal could be obtained on bare graphene region (see Fig. S4 in the supplementary materials).

In the theory of nonlinear optics, SHG originates from the second-harmonic polarization of optical medium induced by the laser electric field.[29] In order to clarify the SHG of Janus MoSSe monolayer, its second-harmonic polarization is determined as (see Note 1 in the supplementary materials)

$$\boldsymbol{P}^{(2)} = \varepsilon_0 \begin{bmatrix} 2\chi^{(2)}_{yzy} E_x E_z - 2\chi^{(2)}_{yyy} E_x E_y \\ -\chi^{(2)}_{yyy} E_x^2 + \chi^{(2)}_{yyy} E_y^2 + 2\chi^{(2)}_{yzy} E_y E_z \\ \chi^{(2)}_{zyy} E_x^2 + \chi^{(2)}_{zyy} E_y^2 + \chi^{(2)}_{zzz} E_z^2 \end{bmatrix}, \quad (1)$$

where $\boldsymbol{E}$ is the laser electric field, $\chi^{(2)}$ is the second-order susceptibility, and ε_0 is the permittivity of free space. The Cartesian indices are defined such that the x-axis is along the zigzag direction, and the z-axis is normal to the layer (see Fig. 1(a)). The four independent nonvanishing tensor elements of $\chi^{(2)}$ are deduced from the crystal symmetry of Janus MoSSe monolayer (C_{3v}) together with the intrinsic permutation symmetry of SHG.[29,31] Equation (1) further reveals that the induced second-harmonic polarization possesses both in- and out-of-plane components. However, the practical detection of SHG

as well as the laser focusing was achieved by an objective with NA<1. The paraxial approximation is therefore appropriate, implying that the $P_z^{(2)}$ would make a minor contribution to SHG signal, and the focused electric field is largely confined in the xy-plane.[32–34] In such scenarios, $\boldsymbol{P}^{(2)}$ is effectively reduced to $-\varepsilon_0\chi_{yyy}^{(2)}\left[2E_xE_y, E_x^2-E_y^2\right] \equiv \boldsymbol{p}^{(2)}$, which is a 2D second-harmonic polarization with $\chi_{yyy}^{(2)}$ as the only contributing susceptibility element.

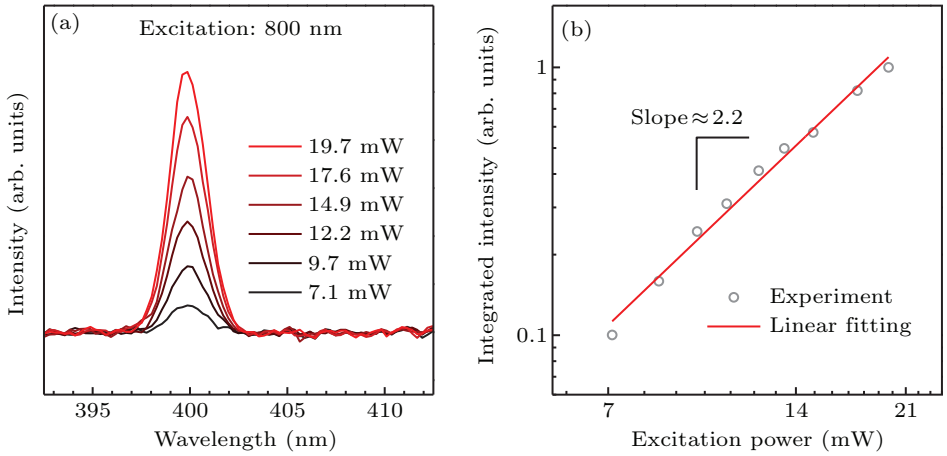

Fig. 2. (a) SHG of Janus MoSSe monolayer under the 800-nm fundamental excitation. (b) SHG intensity as a function of excitation power (plotted on a log–log scale). The slope is extracted from linear fitting.

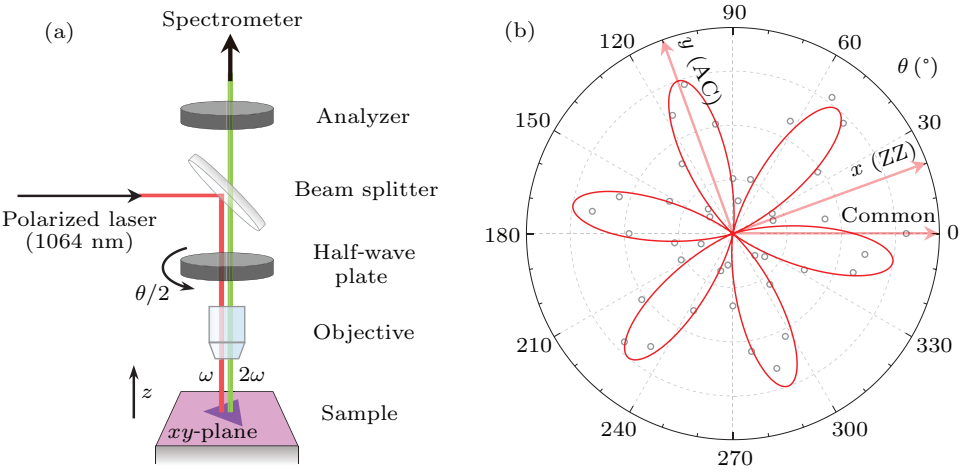

Fig. 3. (a) Illustration of the setup used for the orientation-resolved SHG spectroscopy. The fundamental and second-harmonic paths are represented by the red and green lines, respectively. The half-wave plate is rotated counterclockwise by an angle of $\theta/2$. (b) SHG intensity as a function of θ, measured with the aligned configuration. The red curve with six-fold symmetry is the best fitting to data according to Eq. (3). The zigzag (ZZ) and armchair (AC) directions of the Janus MoSSe monolayer are determined with respect to the common direction (see the red arrowed lines).

Moreover, the dependence of $\boldsymbol{p}^{(2)}$ on the in-plane orientation of Janus MoSSe monolayer enables the orientation-resolved SHG spectroscopy. Our setup, consisting of a linearly polarized excitation laser, a half-wave plate in the common optical path, and an analyzer before the spectrometer entrance, is illustrated symbolically in Fig. 3(a). Based on the Jones calculus of polarization optics,[35] the second-harmonic output has the intensity

$$I_{\mathrm{SHG}} \propto \left| J_{\mathrm{A}} J_{\mathrm{H}} \boldsymbol{p}^{(2)} \right|^2, \tag{2}$$

where J_{A} and J_{H} are the Jones matrices of the analyzer and the half-wave plate, respectively. As for the fundamental path, the laser polarization and hence $\boldsymbol{p}^{(2)}$ are influenced by the rotating half-wave plate. Overall, the angular dependence of SHG intensity is (see Note 2 in the supplementary materials)

$$I_{\mathrm{SHG}}(\theta) \propto \sin^2\left[3\left(\theta+\theta_{\mathrm{L}}\right)-\Phi\right], \tag{3}$$

where θ is twice the rotation angle of the half-wave plate (see Fig. 3(a)), θ_{L} is the angle between the laser polarization and the x-axis, and Φ is a configuration-specific phase. If the laser polarization, the fast axis of half-wave plate, and the pass plane of analyzer are all aligned to a common direction, this phase will vanish. The SHG intensity measured with such an aligned configuration is shown in Fig. 3(b). The six-fold theoretical curve well fits the polarization response. The fitted $\theta_{\mathrm{L}} = -19.9^\circ \pm 0.6^\circ$ determines the zigzag direction of the Janus MoSSe monolayer with respect to the common direction. Also, as evidenced in Eq. (3), the aligned configuration with $\Phi = 0$ allows the direct identification of in-plane orienta-

tion: the maximum of SHG intensity pointing to the armchair direction, while the minimum to the zigzag.

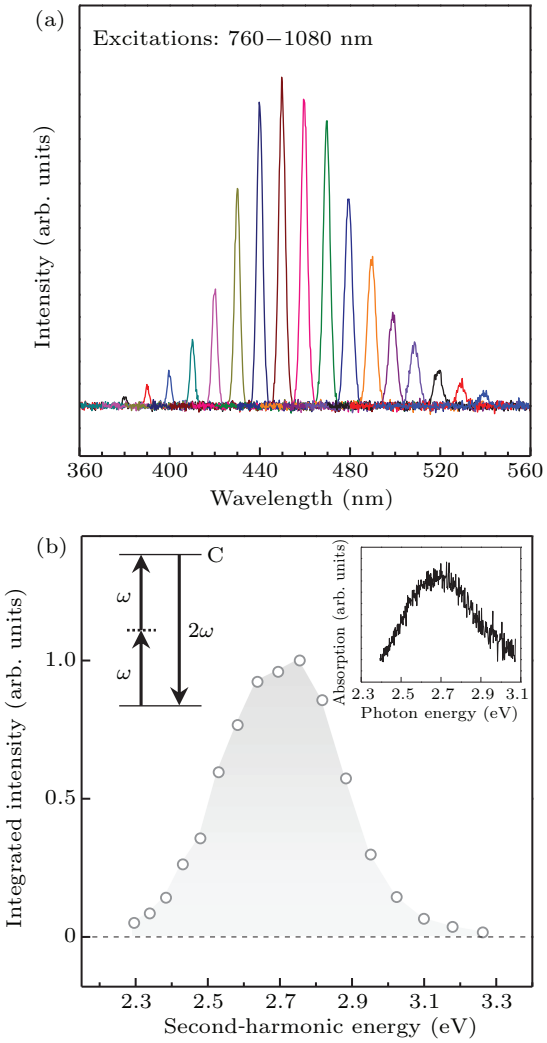

Fig. 4. (a) Wavelength-dependent SHG of Janus MoSSe monolayer. The excitation wavelength was tuned from 760 to 1080 nm, with 20-nm resolution. (b) SHG intensity as a function of second-harmonic energy. Upper-right inset: linear absorption spectrum of Janus MoSSe monolayer measured in the relevant spectral range. Upper-left inset: energy-level diagram illustrating the resonance process. The two-photon transition is resonant with the C-exciton state, which is responsible for the observed SHG enhancement.

Furthermore, the electronic structure of Janus MoSSe monolayer is reflected by the wavelength-dependent SHG spectroscopy. As shown in Fig. 4(a), the excitation wavelength was tuned from 760 nm to 1080 nm with 20-nm steps, and the second-harmonic emission is the most pronounced around 450 nm. The SHG intensity is plotted in Fig. 4(b) as a function of second-harmonic energy. The position of SHG enhancement ($\sim$ 2.7 eV) is coincident with the C-exciton energy of Janus MoSSe monolayer (2.72 eV;[23] also see the upper-right inset in Fig. 4(b) for the linear absorption spectrum, which shows a clear peak at $\sim$ 2.7 eV). This coincidence implies that the two-photon transition is resonant with the C-exciton state, which is illustrated by the energy-level diagram in the upper-left inset of Fig. 4(b).[5,36] The light-matter interaction is particularly strong under resonance, thus the second-order susceptibility becomes large.[29] Specifically, the resonant SHG intensity of Janus MoSSe monolayer is $\sim$ 60 times stronger than the nonresonant value, indicating a nearly eight-fold enhancement of its susceptibility element $\chi^{(2)}_{yyy}$.

4. Conclusion

In summary, we have investigated the SHG of Janus MoSSe monolayer in terms of excitation power, crystal orientation, and exciton resonance. In order to describe the SHG under paraxial focusing and detection, we derive a reduced second-harmonic polarization that lies within the monolayer. Based on this reduced polarization together with Jones calculus accounting for the optical setup, the zigzag and armchair directions of the Janus crystal are quantitatively resolved to an accuracy better than $\pm 0.6^\circ$. Moreover, the SHG intensity is enhanced by a factor of $\sim$ 60 (or nearly eight-fold increase of $\chi^{(2)}_{yyy}$) when the two-photon transition is in resonance with the C-exciton state. Our work unveils the SHG properties of Janus MoSSe monolayer, which may enable novel applications in on-chip optical sourcing and integrated photonic circuits.

Acknowledgements

We thank Wanghua Wu and Yiyang Gong for the assistance with SHG measurements. This work was supported by the National Natural Science Foundation of China (Grant Nos. 61888102, 51771224, and 62175253), the National Key R&D Program of China (Grant Nos. 2018YFA0305803 and 2019YFA0308501), and the Chinese Academy of Sciences (Grant Nos. XDB33030100 and XDB30010000). J. S. and X. L. thank the supports from the National Natural Science Foundation of China (Grant Nos. 20173025, 22073022, and 11874130), the National Key R&D Program of China (Grant No. 2017YFA0205004), the Chinese Academy of Sciences (Grant Nos. XDB36000000 and Y950291), and the DNL Cooperation Fund (Grant No. DNL202016).

References

[1] Corn R M and Higgins D A 1994 *Chem. Rev.* **94** 107
[2] Risk W P, Gosnell T R and Nurmikko A V 2003 *Compact Blue-Green Lasers* (Cambridge: Cambridge University Press)
[3] Zhang J T, Zhao W N, Yu P, Yang G W and Liu Z 2020 *2D Mater.* **7** 042002
[4] Wang Y, Xiao J, Yang S, Wang Y and Zhang X 2019 *Opt. Mater. Express* **9** 1136
[5] Malard L M, Alencar T V, Barboza A P M, Mak K F and de Paula A M 2013 *Phys. Rev. B* **87** 201401
[6] Kumar N, Najmaei S, Cui Q N, Ceballos F, Ajayan P M, Lou J and Zhao H 2013 *Phys. Rev. B* **87** 161403
[7] Janisch C, Wang Y X, Ma D, Mehta N, Elias A L, Perea-Lopez N, Terrones M, Crespi V and Liu Z W 2014 *Sci. Rep.* **4** 5530
[8] Wang G, Marie X, Gerber I, Amand T, Lagarde D, Bouet L, Vidal M, Balocchi A and Urbaszek B 2015 *Phys. Rev. Lett.* **114** 097403
[9] Seyler K L, Schaibley J R, Gong P, Rivera P, Jones A M, Wu S F, Yan J Q, Mandrus D G, Yao W and Xu X D 2015 *Nat. Nanotechnol.* **10** 407

[10] Wu C C, Shang N Z, Zhao Z X, Zhang Z H, Liang J, Liu C, Zuo Y G, Ding M C, Wang J H, Hong H, Xiong J and Liu K H 2021 *Chin. Phys. B* **30** 027803

[11] Mennel L, Furchi M M, Wachter S, Paur M, Polyushkin D K and Mueller T 2018 *Nat. Commun.* **9** 516

[12] Mennel L, Paur M and Mueller T 2019 *APL Photon.* **4** 034404

[13] Liang J, Zhang J, Li Z Z, Hong H, Wang J H, Zhang Z H, Zhou X, Qiao R X, Xu J Y, Gao P, Liu Z R, Liu Z F, Sun Z P, Meng S, Liu K H and Yu D P 2017 *Nano Lett.* **17** 7539

[14] Hong H, Wu C C, Zhao Z X, Zuo Y G, Wang J H, Liu C, Zhang J, Wang F F, Feng J G, Shen H B, Yin J B, Wu Y C, Zhao Y, Liu K H, Gao P, Meng S, Wu S W, Sun Z P, Liu K H and Xiong J 2021 *Nat. Photon.* **15** 510

[15] Li D W, Wei C Y R, Song J F, Huang X, Wang F, Liu K, Xiong W, Hong X, Cui B, Feng A X, Jiang L and Lu Y F 2019 *Nano Lett.* **19** 4195

[16] Qian Q K, Zu R, Ji Q Q, Jung G S, Zhang K Y, Zhang Y, Buehler M J, Kong J, Gopalan V and Huang S X 2020 *ACS Nano* **14** 13333

[17] Chen H T, Corboliou V, Solntsev A S, Choi D Y, Vincenti M A, de Ceglia D, de Angelis C, Lu Y R and Neshev D N 2017 *Light Sci. Appl.* **6** e17060

[18] Fryett T K, Seyler K L, Zheng J J, Liu C H, Xu X D and Majumdar A 2017 *2D Mater.* **4** 015031

[19] Han X B, Wang K, Persaud P D, Xing X Y, Liu W W, Long H, Li F, Wang B, Singh M R and Lu P X 2020 *ACS Photon.* **7** 562

[20] Zhang Z, Zhang L, Gogna R, Chen Z H and Deng H 2020 *Solid State Commun.* **322** 114043

[21] Lu A Y, Zhu H Y, Xiao J, Chuu C P, Han Y M, Chiu M H, Cheng C C, Yang C W, Wei K H, Yang Y M, Wang Y, Sokaras D, Nordlund D, Yang P D, Muller D A, Chou M Y, Zhang X and Li L J 2017 *Nat. Nanotechnol.* **12** 744

[22] Zhang J, Jia S, Kholmanov I, Dong L, Er D Q, Chen W B, Guo H, Jin Z H, Shenoy V B, Shi L and Lou J 2017 *ACS Nano* **11** 8192

[23] Zheng T, Lin Y C, Yu Y L, Valencia-Acuna P, Puretzky A A, Torsi R, Liu C Z, Ivanov I N, Duscher G, Geohegan D B, Ni Z H, Xiao K and Zhao H 2021 *Nano Lett.* **21** 931

[24] Jin H, Wang T, Gong Z R, Long C and Dai Y 2018 *Nanoscale* **10** 19310

[25] Liu X F, Gao P F, Hu W and Yang J L 2020 *J. Phys. Chem. Lett.* **11** 4070

[26] Petric M M, Kremser M, Barbone M, Qin Y, Sayyad Y, Shen Y X, Tongay S, Finley J J, Botello-Mendez A R and Muller K 2021 *Phys. Rev. B* **103** 035414

[27] Mignuzzi S, Pollard A J, Bonini N, Brennan B, Gilmore I S, Pimenta M A, Richards D and Roy D 2015 *Phys. Rev. B* **91** 195411

[28] Guo Y F, Lin Y X, Xie K C, Yuan B A, Zhu J D, Shen P C, Lu A Y, Su C, Shi E Z, Zhang K Y, HuangFu C A, Xu H W, Cai Z Y, Park J H, Ji Q Q, Wang J T, Dai X C, Tian X Z, Huang S X, Dou L T, Jiao L Y, Li J, Yu Y, Idrobo J C, Cao T, Palacios T and Kong J 2021 *Proc. Natl Acad. Sci. USA* **118** e2106124118

[29] Boyd R W 2019 *Nonlinear Optics*, 4th edn. (San Diego: Academic Press)

[30] Zeng J H, Yuan M H, Yuan W G, Dai Q F, Fan H H, Lan S and Tie S L 2015 *Nanoscale* **7** 13547

[31] Wei Y D, Xu X D, Wang S S, Li W Q and Jiang Y Y 2019 *Phys. Chem. Chem. Phys.* **21** 21022

[32] Chu S W, Chen S Y, Chern G W, Tsai T H, Chen Y C, Lin B L and Sun C K 2004 *Biophys. J.* **86** 3914

[33] Wang X H, Chang S J, Lin L, Wang L R, Huo B Z and Hao S J 2010 *J. Opt.* **12** 045201

[34] Yew E Y S and Sheppard C J R 2006 *Opt. Express* **14** 1167

[35] Gerrard A and Burch J M 1994 *Introduction to Matrix Methods in Optics* (New York: Dover Publications)

[36] Trolle M L, Tsao Y C, Pedersen K and Pedersen T G 2015 *Phys. Rev. B* **92** 161409